Electrical Parameters of Nanosecond Dielectric Barrier Discharges (nsDBD)

Martinus Dobbelaar, Delphine Bessieres, Delia Arnaud-Cormos, Philippe Lévêque, Jean H. Paillol

Electrical Parameters of Nanosecond Dielectric Barrier Discharges (nsDBD)

Martinus C. F. Dobbelaar, Delphine Bessieres, Delia Arnaud-Cormos, *Member, IEEE*, Philippe Leveque, *Member, IEEE,* Jean Paillol

***Abstract*— In this study, an electrical device is proposed to generate plasmas in nanosecond dielectric barrier discharge (nsDBD) configuration and to measure the electrical parameters of the discharge over a large bandwidth. Electrical parameters were experimentally determined using a common dielectric barrier discharge equivalent circuit extended here to high frequencies. An efficient synchronization procedure based on a comparison to circuit simulation results was proposed. Discharge current pulses with rise times less than 1 ns and amplitudes up to 50 A were measured. The energy deposited into the plasma and the discharge resistance were determined as a function of time. In addition, circuit simulations support the experimental approach. The nsDBD was accurately modeled by a resistance of the plasma channel following a Rompe and Weizel law in series with a resistance for the discharge spreading along the dielectric surface and a sheath capacitance.**

***Index Terms*— Dielectric barrier discharge, nanosecond pulsed electric fields, electrical parameters characterization.**

I. INTRODUCTION

Nanosecond pulsed electric fields (nsPEF) is a promising technique in biomedical applications such as cancer treatment [1]–[6]. New trends consist in applying high voltage pulses with ultra-short durations of a few nanoseconds and intense electric field strength up to tens of megavolt per meter. For applying nsPEFs [7], [8], a technique described in [9], [10] consists in exposing without direct contact with a biological sample placed into a guided transverse electromagnetic (TEM) structure.

Non-thermal plasmas on the same nanosecond time scales are explored for similar biomedical investigations purposes [11]–[13]. Recent developments of dielectric barrier discharge devices operating with nanosecond (nsDBD) high voltage pulses particularly demonstrated potential capabilities for cancer therapy [14].

NsDBD can be ignited within gaps of approximately 1 mm, filled with atmospheric pressure air at natural humidity. One condition for radially uniform discharge ignition is applying voltage pulses with sufficient sharp rise times i.e. shorter than 1 kV/ns [13], [15], [16]. Uniformity of the discharge was found to be dependent on the applied field [14], [17]. For high electric fields, camera recordings show that discharges are generated over in the entire gap area, whereas at low fields, discharges consist of several parallel channels within the gap [14], [18], [19]. nsDBDs were also studied by optical emission spectroscopy to investigate both space and time resolved development of the reduced electric field [14]. In this latter study, nsDBD operated under high voltage pulses with amplitude of several tens of kV, rise times between 1.6 ns and 2.2 ns and a duration of 12.3 ns. Measurement of time scale electrical parameters of nsDBD is challenging due to the high-voltage levels and the nanosecond time scale variation of discharge currents.

In this context, the aim of this work is to propose an experimental setup and technique allowing to combine and generate both nsPEF and nsDBD. The experimental conditions of discharge generation are similar to those used in [14]. The present study focuses on the generation of nsDBD, measurement techniques and electrical characterizations of discharge.

To electrically characterize DBDs, parameters are commonly determined based on an equivalent circuit of the inter-electrode system [20]. Two capacitors modeling the air gap and the dielectric layer were considered in series. This model initially proposed to determine the power consumption by voltage versus charge Lissajous figures [21] has been extended by Liu and Nieger [22]. The discharge is electrically represented by a current source accounting for the ohmic discharge current in the gas gap. The authors applied this model to sub-microsecond unipolar voltage pulses in [22] and proposed an extension to all sources in [23]. Based on Liu and Nieger's, Shao *et al* [24] also showed that this equivalent circuit allows the experimental determination of nsDBD electrical parameters. A calculation of the transient power delivered by the electrical circuit as a function of time was also proposed in [24]. Electrical models of dis-

Manuscript submitted April 26, 2021;

M. C. F. Dobbelaar is with University of Pau and Pays de l'Adour, E2S UPPA, SIAME, Pau, France and University of Limoges, CNRS, XLIM, UMR 7252, F-87000 Limoges, France.

D. Bessières, J. Paillol are with the University of Pau and Pays de l'Adour, E2S UPPA, SIAME, Pau, France. (*Corresponding author: Jean Paillol, jean.paillol@univ-pau.fr*).

D. Arnaud-Cormos is with the University of Limoges, CNRS, XLIM, UMR 7252, F-87000 Limoges, France, and also with the Institut Universitaire de France (IUF), 75005 Paris, France.

P. Leveque is with the University of Limoges, CNRS, XLIM, UMR 7252, F-87000 Limoges, France.

charges were also proposed for filamentary or homogeneous regimes of DBD, respectively in [25], [26].

However, classical DBD regimes differ from nsDBD regime because of the high over-voltages and short formative time lags of few ns. Under these conditions, the discharge current pulse amplitude is of tens of amps and the rise time in the ns range. Electrical models of discharge were developed for the ns regime in [27]. However, in [27] the discharges presented were developing between parallel metallic planes without considering a dielectric layer. In these conditions, the authors found that a resistance, which non-linearly depends on the current, can suitably model the discharge channel.

In this study, we present an experimental device for nsDBD electrical parameters measurements over a large bandwidth. The electrical measurements are conducted for a single shot discharge. We electrically characterize the nsDBD by using the Liu and Nieger [22] equivalent circuit of the dielectric barrier electrode system that we extend to high frequencies. We include an electrical model of the nsDBD. In addition to these experimental results, we propose a full circuit simulation including a discharge model resistance to model the experimental approach. Section II presents the experimental setup and measurements systems for nsDBD generation and characterization. In section III, an electrical analysis of the discharge model, based on a synchronization procedure fitting circuit simulation and measurement results, is proposed. Experimental results and circuit simulation of the discharge electrical parameters are presented in section IV.

II. Experimental setup and Measurement systems

A. Experimental device

The experimental device presented in Fig. 1 was specifically designed for application of a nanosecond high voltage pulses to a discharge cell. All components were designed with a 50 Ω impedance and HN connectors. Indeed, a 50 Ω matched circuit is preferred as the voltage applied to the discharge cell can be directly measured and electromagnetic interferences are reduced. All waveforms are displayed on a 3 GHz bandwidth oscilloscope (DSO, TDS 694C, Tektronix, USA) presenting a sample rate of 10 GS/s. To prevent over voltages, high-voltage attenuators (Model 142, Barth Electronics Technology, USA) are connected to each oscilloscope input (A, B and C).

The pulse generator (FPG 10-1SM10 FID Technology, Burbach, Germany) is connected to two outputs via a Tee adaptor (PE9575, Pasternack, USA) i.e. a three port devices that is used to split the signal with three 50 ohms connectors. One output is a 50 Ω matched load composed of a high-voltage attenuator connected in series to oscilloscope input A. The second output is directly connected to the discharge cell, corresponding to an open circuit in the absence of the discharge. Thus, the main innovation of the setup consists in implementing in parallel to the discharge cell a circuit matching the impedance load and allowing pulses measurement. The pulse generator delivers 14 ns duration pulses with 4.4 ns rise time and an adjustable voltage amplitude up to 10 kV.

The setup components are connected through coaxial cables

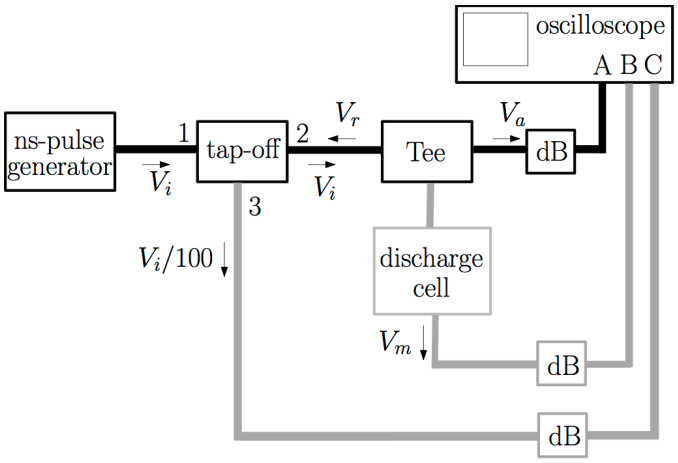

Fig. 1. Schematic of the experimental set-up. The main circuit composed of the pulse generator, the tap-off, the tee adaptor and the oscilloscope is represented in dark black. V_i and V_r are the incident and reflected voltage pulses, V_a is the voltage pulse applied to the discharge cell. V_m is the measured voltage across the discharge cell. $V_i/100$ is the voltage measured by the tap-off (port 3) system with a ratio of 100.

(RG214, Multicomp Pro, USA). The propagating voltage pulses in the circuit are measured via a tap-off (Model 241, Barth electronics, USA) placed between the generator and the Tee adaptor [28]. The tap-off consists in a voltage divider of ratio 1/100 between port 1 and port 3 (Fig. 1). The risetimes for the mainline (ports 1 and 2) and for the measurement port 3, are 30 ps and 1.5 ns, respectively. This component has the right bandwidth or calibration over the entire parameter range of our measurements. To separate incident and reflected pulses, long coaxial cables are inserted in the setup. The length of the cables between the tap-off and Tee adaptor/discharge and between the pulse generator and the tap-off are 5.18 m and 3 m, respectively. All cables connecting to the oscilloscope are 1 m long. In Fig. 1, V_i is the voltage pulse delivered by the generator which propagates towards the Tee adaptor. Note that the connection between the Tee and the discharge cell is short enough to prevent from any additional reflections due to its length. The discharge cell represents the main cause of impedance mismatching in the circuit, particularly at high frequencies. Therefore, a reflected voltage V_r is generated which propagates backwards toward the generator. V_a is the voltage applied to the discharge cell and it corresponds to the sum of the incident and the reflected voltages i.e., $V_a = V_i + V_r$.

The discharge current pulse is measured across a measurement resistor placed in series with the discharge cell. In practical terms, the resistor corresponds to the 50 Ω input impedance of the oscilloscope in series with an HV attenuator (oscilloscope B input on Fig. 1). The measured current is computed as $V_m/50$, where V_m is the measured voltage. This technique, commonly used for low frequency measurements [29], [30], was successfully extended in [31] to characterize Nanosecond Repetitive Pulse Discharges (NRPDs) current pulses in a point-to plane electrodes configuration.

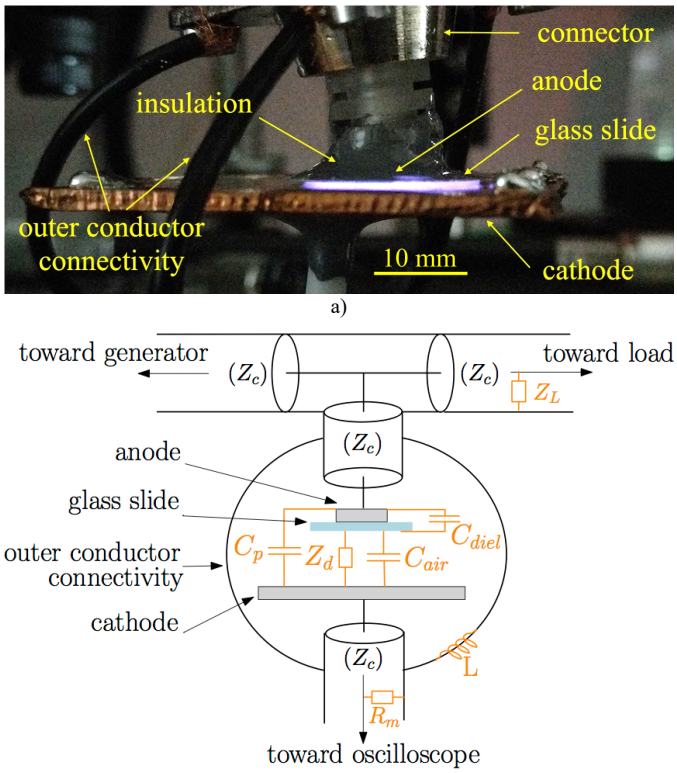

Fig. 2. nsDBD cell (side view), a) picture and b) schematic. The picture of discharge was acquired during a 10 s exposure time. The discharge conditions for a 1 mm air gap distance were: an incident voltage pulse magnitude of 10 kV with a repetition rate frequency of 10 Hz. The cable characteristic impedance Z_c is 50 Ω. The electrical elements modelling the circuit are represented in orange.

B. Discharge cell

The discharge cell is represented in Fig. 2. The anode is a thin metallic film disk of 0.75 cm radius connected to the inner conductor of the HN connector (R176404, Radiall, France). The anode is made with an copper ribbon adhesive to the glass. The upper part of the copper ribbon is glued to the HN connector using a conductive epoxy (CW2400, Circuit Works, USA). The dielectric layer is a glass slide disk with a relative permittivity of 7, a 140 µm thickness and a 1.1 cm radius. To ensure complete electrical insulation, the dielectric disk radius is greater than the high voltage electrode radius. An insulating resin (EA3450 Loctite, Henkel, Germany) was added upon the anode electrode to prevent surface discharge over the glass at anode edges. The cathode, which is a 20 cm^2 squared copper plate, is connected to the inner conductor of an SMA (R125414, Radiall, France) connected to an attenuator in series to oscilloscope input B. The material and thickness of the dielectric layer were selected to ensure a high capacitance and to enhance the voltage drop across the air gap. To ensure the continuity of voltage potential reference, four bonding wires were attached to the outer conductors of the two connectors. The air gap distance was 1 mm.

The discharge cell, i.e., the delivery device, was customized for further exposures of biological cells contained in biological solutions inside Petri dishes. Indeed, a Petri dish can be directly

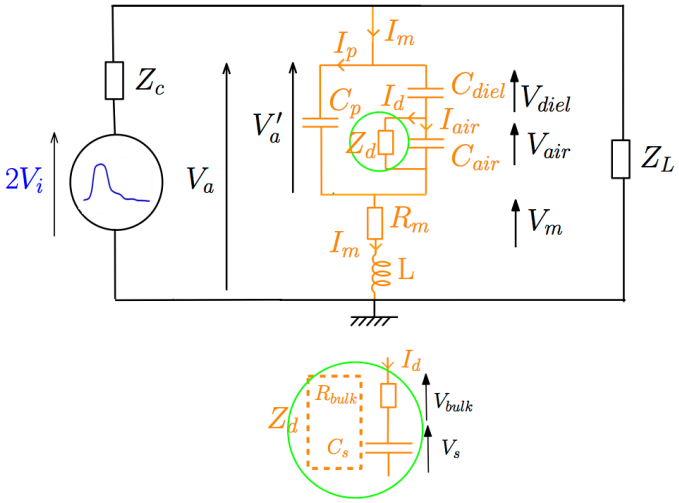

Fig. 3. Setup of the equivalent circuit. The main circuit is drawn in black while the discharge cell and stray elements are reported in orange. The discharge impedance $Z_d(t)$ components, circled in green, are detailed.

set on the cathode metallic plane. As illustrated Fig. 2, discharges can develop in the air between the biological solution surface and the glass slide dielectric. The delivery device is optimized for biomedical applications in terms of dimensions, voltage polarity and prevention of electromagnetic interferences. The detailed Petri dish modelling and impact on the discharge parameters will be the focus of a separate paper. As required for medical applications, air relative humidity RH is close to 100% during experiments.

III. Electrical Analysis

To characterize the electric behavior of the discharge cell, an equivalent circuit is proposed. Electrical characterization of DBDs classically consists in determining the discharge current, the voltages across the air gap and the dielectric layer, and the energy deposited in the plasma. All of these parameters cannot be directly measured therefore they are determined on the basis of the measured voltage applied to the discharge cell and the measured current.

A. Circuit model

The electrical elements are displayed on Fig. 2 (b) and the corresponding equivalent electrical circuit is proposed on Fig. 3. The proposed scheme is based on the classic DBD equivalent circuit proposed by Liu and Neiger [22]. It involves two capacitors in series, modelling the air gap where the discharge develops (C_{air}) and the dielectric layer (C_{diel}). The discharge is symbolized by a time dependent impedance $Z_d(t)$ [21]. A naturally existing stray capacitance (C_p) between the two electrodes is added in parallel to the components (C_{air}, C_{diel}) [26]. Outer conductor connectivity was specifically designed to reduce the capacitance between the anode and the ground. This capacitance is assumed to play a minor role in our configuration and is thus neglected. The circuit is completed by a stray inductance L, for connections modeling at high frequencies, in series with

and a measuring resistance R_m. The voltage generator is modeled by a voltage supply delivering ($2 \times V_i$) in series with a 50 Ω output resistance (Z_c). The generator is loaded by a 50 Ω matching impedance Z_L. The discharge impedance (zoom in Fig. 3), consists in a current driven nonlinear resistance (R_{bulk}) in series with a capacitor (C_s). The discharge model is further detailed in sub-section C.

Applying Kirchoff's laws to the circuit presented in Fig. 3 allows the calculation of the electrical parameters based on two measured data i.e V_a and I_m. Let's define the voltage V_a' as directly applied to the inter-electrode system without considering parasitic self-inductance effect nor measuring resistance. V_a' is obtained as:

$$V_a^{'} = V_a - R_m I_m - L\frac{dI_m}{dt} \quad (1)$$

According to the equivalent circuit of Fig. 3, the electrical parameters (V_{diel}, V_{air}, I_d) are expressed as a function of time by:

$$V_{diel}(t) = \frac{1}{C_{diel}}\int_0^t I_m(\tau)d\tau - \frac{C_p}{C_{diel}}V_a^{'}(t) \quad (2)$$

The dielectric layer is considered uncharged as a single shot discharge is generated. As a consequence, $V_{diel}(t=0) = 0$ V.

$$V_{air}(t) = \left(1 + \frac{C_p}{C_{diel}}\right)V_a^{'}(t) - \frac{1}{C_{diel}}\int_0^t I_m(\tau)d\tau \quad (3)$$

$$I_d(t) = \left(1 + \frac{C_{air}}{C_{diel}}\right)I_m - \left(C_p + C_{air} + \frac{C_p C_{air}}{C_{diel}}\right)\frac{dV_a^{'}}{dt} \quad (4)$$

The energy deposited into plasma is an important parameter for applications and is commonly calculated by considering the losses in measuring resistance R_m:

$$E_1 = \lim_{t\to\infty}\int_0^t (V_a(\tau)I_m(\tau)d\tau - R_m I_m^2(\tau))d\tau \quad (5)$$

Equations (2)-(5) depend on the values of the electrical elements (C_{air}, C_{diel}, C_p, L) assessed in the next sub-section.

B. Circuit elements assessment and waveforms synchronization, without discharge

Capacitances C_{air} and C_{diel} are calculated by using the standard formula :

$$C = \frac{\varepsilon_0 \varepsilon_r S}{e} \quad (6)$$

If we consider S being the surface of the anode electrode, ε_r the relative permittivity and e the gap length, the value of the air gap capacitance C_{air} is approximately 1.8 pF (S = 1.77 cm^2, $\varepsilon_r = 1$, e = 1 mm). C_{diel} is similarly obtained for the dielectric layer capacitance and its value is 80 pF (S = 1.77 cm^2, $\varepsilon_r = 7$, e = 140 µm).

Parasitic capacitance C_p and stray inductance L can only be determined by circuit simulation using a fitting procedure with experiments. A specific circuit simulation was developed to model the experimental approach. The circuit model is based on the electrical schematic in Fig. 3. The set of differential equations of Kirchoff's laws are solved by implicit finite difference technique. The system of equations is solved by a linear algebra technique requiring a dense matrix inversion [32]. The simulation discretization time is given by experimental sampling period. The delivered voltage pulse V_i is given by the tap-off measurement (Fig. 2). For noise reduction, V_i signal is filtered by a numerical moving average filter over 5 points with a sampling period of 0.1 ns.

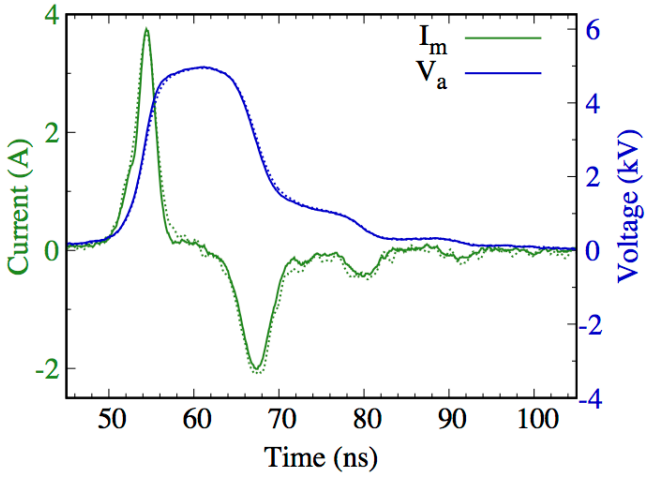

Fig. 4. Voltage and current pulses without discharge for a 5 kV incident voltage pulse. Applied voltage V_a in blue and measured current I_m in green. Measurements are in solid lines and computed results are in dotted lines.

TABLE I
OPTIMIZED CIRCUIT ELEMENT VALUES

C_{diel} (pF)	C_{air} (pF)	C_p (pF)	L (nH)
80	1.8	1.1	41.1

To prevent any discharge activity during measurements, the supplied voltage V_i is set to 5 kV. Applied voltage V_a and measured current I_m obtained in experiments and simulation are presented in Fig. 4. The applied voltage V_a has a full width duration at half magnitude (FWHM) of 13.8 ns and a rise time of 4.4 ns. The measured current presents a classical shape of a displacement current through a capacitor with a maximum amplitude of of 3.8 A.

By convention, time t = 0 is defined at the beginning of the supplied V_i voltage recording. An efficient synchronization procedure is necessary for an accurate determination of the discharge parameters. Experimental current and voltage waveforms are synchronized by comparing experiments to simulation results. Experimental results are time shifted to fit with simulation data. This procedure is particularly efficient because of the good agreement between experimental and simulation results. Synchronization accuracy is then estimated at one discretization time period (0.1 ns).

Modeling is performed with parameters values that are shown

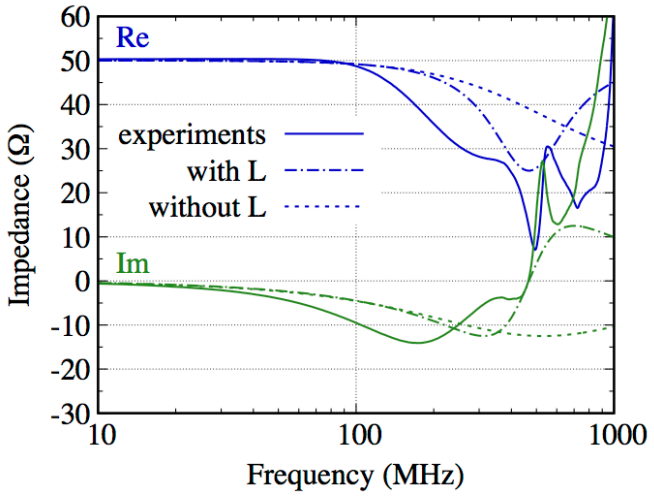

Fig. 5. Equivalent impedance of the cable termination including the discharge cell and the matching load. Experimental results computed from the S_{11} measurements are in solid lines and theoretical results with or without the stray inductance in the electrical circuit are in dotted lines. The air gap distance was 1 mm.

in Table I. To obtain the optimized values of C_p and L, simulated results are fitted with experimental ones. The capacitance C_p can then be estimated by simple fitting with measured current I_m and applied voltage V_a. In contrast, inductance L cannot be accurately determined in transient domain. Its role being very predominant at high frequencies (> 100 MHz), its value is determined by a fitting procedure in the frequency domain.

To perform an experimental frequency analysis, a vector network analyzer (VNA, 8753E model from Hewlett Packard, USA) was connected instead of the pulse generator at the Tee adaptor input. The VNA allowed measuring S_{11} reflection coefficient as a function of frequency. The equivalent impedance consisting in the matching load Z_L in parallel to the discharge cell is calculated from S_{11} parameter. Real and imaginary parts of the equivalent impedance are plotted in Fig. 5. As observed, the impedance is mainly resistive (50 Ω) at frequencies lower than 100 MHz. Mismatching is due to the discharge cell set in parallel to the Z_L matching load. As the frequency increases, the real part of the impedance progressively decreases from 50 Ω to 7 Ω at 500 MHz and the imaginary part decreases down to −14 Ω at 180 MHz. The negative imaginary part is due to the discharge cell capacitive behavior. A series resonance occurs at 470 MHz. The equivalent impedance becomes positive beyond and the impedance can be related to an inductance.

Simulation results of the equivalent impedance are performed with or without the stray inductance. Experiments are compared to simulation obtained with the optimized electrical elements of Table I. When considering the stray inductance, the numerical model accurately reproduces the experimental results up to 470 MHz, i.e., the resonance frequency. In practice, the series resonance is obtained for a stray inductance L value of 41.1 nH. If no inductance is considered, the equivalent impedance model is accurate only for frequencies below 200 MHz. It can be concluded that the stray inductance is of particular relevance to extend the validity of the model up to 700 MHz.

As a conclusion, the Liu and Neiger [22] DBD equivalent circuit in combination with a parasitic capacitance and a stray inductance is validated under nanosecond pulse excitation. Under this condition, the circuit presented in Fig. 3 accurately models the experimental setup and allows an accurate experimental waveforms synchronization. This electrical circuit will be used to characterize the discharge.

C. Discharge parameters

Discharge ignition induces a rapid increase of the discharge current, typically in the nanosecond range, particularly for high over-voltage configurations [33]. Ionization in the air gap and sheaths formation governs the discharge development in its first steps. To model the discharge, a capacitor for the sheath capacitance (C_s) in series with a resistor (R_{bulk}) as the plasma channel equivalent resistance is proposed. This model is extracted from [34], [35] where discharges are modeled under radiofrequency signal excitation. The discharge is considered as uniform in the transversal direction as a first simplified approach that provides however satisfactory results in the discharge electrical parameters determination.

Assuming valid the (C_s , R_{bulk}) model, the voltage (V_{bulk}) across R_{bulk} is calculated as an experimentally determined parameter:

$$V_{bulk}(t) = V_{air}(t) - \frac{1}{C_s}\int_0^t I_d(\tau)d\tau \qquad (7)$$

Although the sheath capacitance C_s varies with time as the discharge develops [36], its value is considered constant as a first approximation. C_s value is determined by a fitting procedure which assumes that (I_d) and (V_{bulk}) vary similarly and that they consequently present the same polarity. Hence, they should both change sign at the same time. Measurements quality and the synchronizing procedure control are necessary to accurately determine C_s value. The nsDBD studied in the paper correspond to single shot discharges ignited after a delay. The measured current is not dependent on the delay and therefore, the dielectric charge is neglected in Eq (7).

The V_{bulk} value is determined in a post-processing procedure once $I_d(t)$ and $V_{air}(t)$ are calculated.

The bulk resistance is then determined by:

$$R_{bulk}(t) = \frac{V_{bulk}(t)}{I_d(t)} \qquad (8)$$

As a final step, the energy deposited in the discharge can be calculated by:

$$E_2 = \lim_{t\to\infty}\int_0^t V_{bulk}(\tau)I_d(\tau)d\tau \qquad (9)$$

Discharge energy can be calculated using (eq. 5) or (eq. 9). If we consider that losses in the circuit are mainly due to the discharge losses then E_1 (eq. 5) and E_2 (eq. 9) are equal. For energy assessment validation, this equality is verified for all set of measurements.

D. Model of discharge resistance and circuit simulation

In addition, a model of discharge resistance is proposed for

validation. The resistance model is integrated in the circuit for full numerical simulation. Kirchoff's equations are numerically solved by the technique introduced in section III-B. The only input parameter of the simulation is $V_i(t)$.

Numerous models were proposed for discharge channel resistance determination [27]. Theoretical modeling of switching processes on nanosecond time scale were examined in [37]. The studies show that in over-voltage conditions the Rompe and Weizel theory [38] produce accurate results. The model proposes that the discharge is mainly governed by ionization process inducing plasma channel conductivity variation over time. In the time scale under consideration, no hydrodynamic expansion is assumed. Thus, the theory assumes that the energy deposited in the plasma is transferred to electrons through ionization only.

The dynamic discharge resistance (R_{RW}) based on Rompe and Weizel [38] theory is given by:

$$R_{RW}(t) = \frac{2h}{\sqrt{2a_i \int_0^t I_d^2(t)dt}} \qquad (10)$$

where a_i is an energy parameter (m^2/V^2s) derived from ionization process, h is the channel length (m), t is time (s) and I_d is the discharge current (A). Parameters h and a_i are supposed to be time independent as it is experimentally shown in similar conditions in [39]. Equation 10 implies a constant electric field along the channel and a cylindrical plasma uniformity.

$R_{RW}(t)$ models the nsDBD within a volume. However, nsDBD also spreads along the dielectric surface which is perpendicular to the applied electric field [15]. Thus, the energy deposited into the plasma is the sum of the energy deposited within the volume and along the dielectric surface. An additional series plasma resistance (R_a) is then proposed to model the energy loss in the plasma which develops along the surface. As a first approach, R_a value is assumed to be independent on the discharge current therefore it has to be determined by comparison with experiments for each discharge. R_a can be considered as a requisite fitting parameter in the dynamic discharge resistance determination. The complete dynamic resistance is thus computed as:

$$R_d(t) = R_{RW}(t) + R_a \qquad (11)$$

Both a_i (eq. 10) and R_a (eq. 11) are considered as parameters of the model. Parameter a_i influences the time delay to discharge ignition and the current rise time while R_a mainly affects the current amplitude. Their values are determined by fitting simulation results to experiments. As a consequence, this $R_d(t)$ model is valid for a given set of experiments. In the following, numerical results are obtained by replacing R_{bulk} by R_d in circuit simulation.

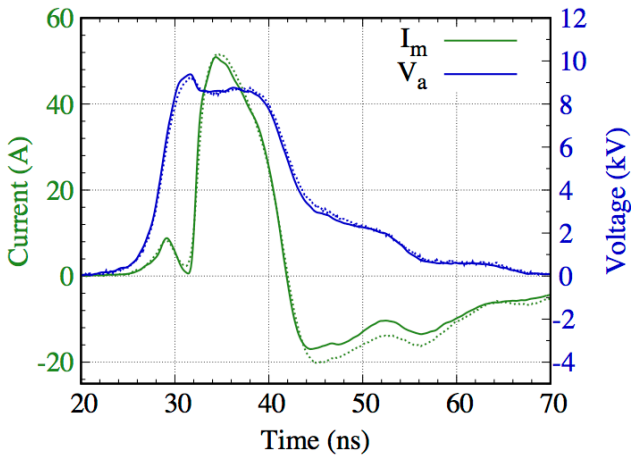

Fig. 6. Measured current I_m (green) and applied voltage pulse (blue). Experimental data are in solid lines and simulation results in dotted lines. Results are obtained on the basis of the optimized elements given in Table 1. Parameters of the discharge modelling are: ai = 2.6 10^{-4} m^2/V^2s, R_a = 35 Ω and C_s = 285 pF.

IV. Results

A. Discharge ignition conditions

A discharge activity is identified by the measurement of a significant additional current observed in our conditions for pulse voltages higher than 6.9 kV. At this threshold, the discharge pulse amplitude is approximately 6 A with an ignition delay of 11.3 ns. If the applied voltage is increased to 10 kV, a discharge current pulse is consistently recorded. The maximum discharge pulse amplitude increases up to 55 A. One typical pulse obtained at 9.5 kV applied voltage value is considered in this study. For this pulse, with lower voltage levels close to the ignition threshold, measured discharges mainly differ in amplitude level while current rise times have rather similar values. For a given applied voltage, discharges and associated electrical measurements are very reproducible. The discharge develops in the air gap between the cathode and the dielectric surface. It visually occupies the entire gap (see in Fig. 2a)). The delay to ignition is reduced and the discharge starts when the voltage pulse attains its maximum value. No significant jitter in the delay of the discharge current pulse is observed. The applied voltage is at least three-fold the breakdown voltage (2.8 kV). At such over-voltage levels, the formative time lag is estimated to be less than 1 ns. A discharge can ignite only if the ignition delay is shorter than the pulse duration. As the humidity level increases, time lags, dispersion of discharge pulses amplitude and delays are reduced [35].

B. Measured current and applied voltage

Raw experimental data of the measured current I_m and the applied voltage V_a are compared to optimized simulation results in Fig. 6.

In experiments, the amplitude of the voltage delivered by the pulse generator is 9.5 kV. When observing I_m, the maximum currents of 9 A at 29 ns and 51 A at 32.5 ns are attributed to the displacement current and the discharge activity, respectively.

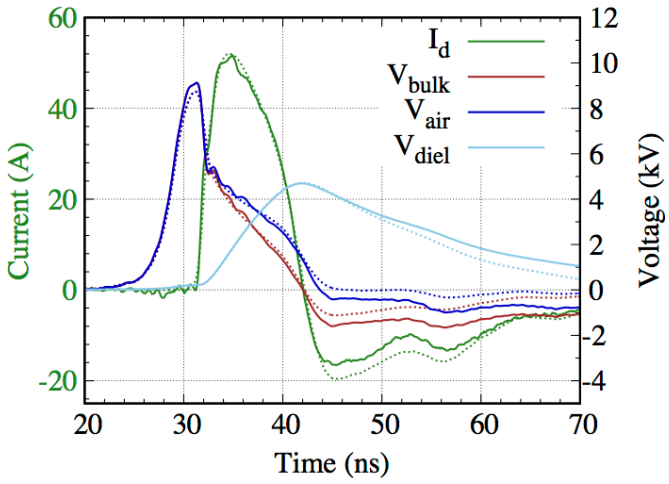

Fig. 7. Discharge current I_d (green). Voltage pulse applied to the air gap V_{air} (blue). Applied voltage to the plasma bulk V_{bulk} (red). Voltage applied to the dielectric layer V_{diel} (cyan). Experimental data are in solid lines and simulation results are in dotted lines.

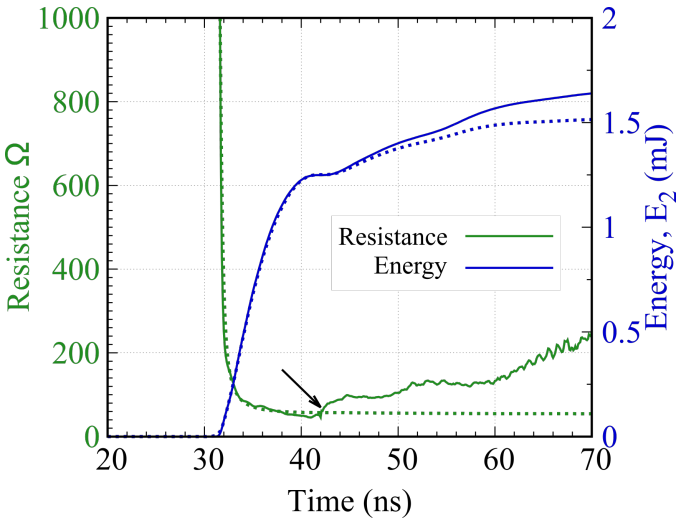

Fig. 8. Dynamic discharge resistance (green) and energy of the discharge (blue) as function of time. Experiments using R_{bulk} are in solid lines and simulation using R_d in dotted lines.

The rise time of the current pulse is 1.4 ns. The discharge becomes negative reaching −17 A at 44 ns during the applied voltage fall time and then tends toward zero after the pulse ending. The V_a voltage amplitude drop of approximately 700 V at 32.5 ns is attributed to impedance mismatching due to discharge ignition. The discharge cell impedance is then lowered by the weak discharge channel resistance thus inducing a reflected voltage pulse V_r. This mismatching has already been described in ns pulsed discharge simulations [40]. Note that less than 5% of the incident pulse voltage is reflected backwards the generator by the discharge cell due to the 50 Ω matching.

In simulation, while the applied voltage V_a presents an overall good level of consistency, the current I_m is slightly overestimated beyond 42 ns compared to experimental measurements. However, it can be concluded that an overall accurate fitting is obtained with considered optimized values a_i of 2.6 10^{-4} m^2/V^2s and R_a of 35 Ω. Jobava et al [27] found current values and time frames typical for electrostatic discharges (ESD). ESD electrical parameters are very close to nsDBD parameters presented in this paper. The ai coefficient has been experimentally determined for various gap lengths and applied voltages in [27] with values in the interval 2 to 3.5 10^{-4} for a 1 mm air gap and an applied voltage of 10 kV. Thus, the ai value in our configuration is consistent with measured data found in [27]. These results support the proposed equivalent circuit and discharge models.

C. Discharge current and voltages

The discharge current pulse presented in Fig. 7 is experimentally determined using equation (4). The pulse starts at 32.1 ns and its shape is similar to the current pulse (t > 32 ns) revealed in the measured current Fig. 6. The main difference consists in a hump in the leading edge. The discharge current reaches 29 A at 32.1 ns with a rise time of 0.5 ns and then continues to increase with a rise time of 0.7 ns. Based on the proposed electrical model, the first pulse rise time is due to the discharge of the air gap capacitor C_{air} into the discharge resistor. The second rise time is due to the parasitic capacitance C_p and the measure circuit (R_m, L).

The voltage across the air gap is given by equation (3). As observed from Fig. 6 and 7, V_{air} is no longer identical to V_a after 32.1 ns. V_{air} amplitude decreases due to the discharge ignition and mismatching. Between 32.1 ns to 42 ns, the sheath capacitor is charged by the discharge increasing the voltage across the layer V_{diel}. As V_{diel} reaches a maximum of 4.5 kV at 42 ns, V_{air} becomes negative and consequently the discharge current sign changes. Note that V_{diel} is still significant (1 kV) at the end of the applied voltage pulse. The charge of the dielectric on a time scale superior to the duration of the applied voltage pulse is responsible for a residual discharge current (-4 A at 70 ns).

The voltage across the sheath subtracted to V_{air} gives the voltage drop across the resistive part of the discharge V_{bulk} (eq. 7, Fig. 7). In these conditions, the optimized sheath capacitance C_s is the value for which the voltage across the plasma bulk is in phase with the discharge current. Specifically, C_s is the capacitance value allowing V_{bulk} and I_d to cross zero axis at the same time. This is obtained at 42 ns for C_s equal to 285 pF. The sheath voltage increases as long as the discharge current remains positive. At 42 ns, the current becomes negative and the sheath fall voltage attains its maximum amplitude of 1.3 kV.

Simulation results are also presented in Fig. 7. The comparison with experimental results shows a good agreement particularly up to 42 ns. Beyond this value, in simulation voltages are underestimated and currents are overestimated by approximately 10% compared to experiments. Slight differences appear when the discharge current is negative. Note that the parameters of the discharge model are optimized for high voltages leading to ionization process and currents of tens of A. They are consequently less efficient towards the applied pulse end at low level voltages and currents. Moreover, Cs may change with polarity and this could explain the difference beyond 42 ns. Indeed, as current switches from positive to negative values, the cathode sheath does not exist anymore in the vicinity of the me-

tallic plane. The evolution of the sheath with the change of current polarity at the dielectric surface is not modelled in our configuration. Simulation results nevertheless remain fairly close to experiments and the efficiency of the electrical discharge modeling is validated.

D. Dynamic resistance and energy of the discharge

The experimental dynamic resistance given by equation (8) is plotted in Fig. 8. The discharge ignition at 32 ns induces a significant rapid decrease of the resistance from arbitrary huge chosen values down to 200 Ω in 0.5 ns. This corresponds to the first rise time of the discharge current pulse before the hump in the leading edge. During the following 0.7 ns, i.e., the second rise time of the current pulse before the maximum peak, the resistance slowly decreases to 70 Ω. Up to 42 ns, the resistance is approximately constant with a 54 Ω mean value. At 42 ns (arrow in Fig.8) as the current changes to negative polarity, the resistance starts to increase. In case of metallic electrodes conditions without dielectric layer, the discharge resistance values are in the order of several Ω [41], [42]. The higher resistance in case of one electrode covered by dielectric is attributed to the discharge spreading along the dielectric surface which prevents sparking. As the voltage applied to the bulk resistor decreases from 42 ns, discharge resistance continuously increases up to a value of 220 Ω. Final resistance values from 60 ns to 70 ns, with amplitudes up to 200 Ω are noisy due to the low current values.

To compare with experiments, simulation results are also plotted in Fig. 8. Both results of the discharge resistance present a good agreement up to 42 ns. Thus, the association of a resistance obeying Rompe and Weizel formulation in series with a constant resistance can accurately model the discharge formation and development. Beyond 42 ns, the applied field to the discharge plasma is lower than the critical field of 28 kV/cm. Therefore, ionization process cannot be the leading process in the gap. The slow recombination process in the gas and at the electrodes cannot be fully taken into account, thus limiting the proposed model. However, note that voltages and currents at low field can be roughly estimated in spite of the resistance approximation.

The energy deposited in the discharge plasma as a function of time (Fig. 8) requires energy calculation with equation (9) and a complete electrical circuit analysis. During 6 ns after discharge ignition, the energy is linearly varying with time with a slope of 180 µJ/ns. The energy then reaches a plateau value of 1.2 mJ, followed at 42.1 ns by an increase due to the negative current with a flatter slope (10 µJ/ns). The energy tends to a limit value of 1.67 mJ. Note that 70% of the limit value is deposited in the first 6 ns of the discharge. The energy is thereafter limited by the conductivity increase of the discharge channel. The calculation of the limit value of the energy using equation (5) results in a value of 1.71 mJ, nearly the value obtained by eq. 9. Equation (5) is based on direct measurements and only gives the total energy deposited into plasma. This energy value is in agreement with the energy per voltage pulse measured in similar conditions [12], [14].

As for the resistance, the simulation (Fig. 8) of the energy deposited into the discharge channel agrees with experiments up to 42 ns with some slight differences beyond. An overall agreement is however obtained, since the energy is mainly deposited in the first steps of the discharge where fields are superior to the critical field.

V. Conclusions

In this paper, an electrical device for nsDBD generation was proposed. Voltage and current measurements over a large bandwidth are included in the setup. Electrical characterization of the discharge was performed in conditions that are suitable for future exposures of biological samples.

To characterize the nsDBD, the classical Liu and Neiger's equivalent circuit was extended to high frequencies. One additional parasitic capacitor between the two metallic electrodes was added in the model. A self-inductance accurately modelled electrical connections. The challenging issue of waveforms synchronization was solved by numerical circuit simulation and comparison to experiments.

An electrical model of nsDBD was proposed and included in the equivalent circuit. It consisted of a pure resistance to model the plasma channel and a sheaths capacitance. The voltage and the discharge current pulses were experimentally determined. The rise times of the current pulse were 0.5 ns and 0.7 ns before and after the hump, respectively. A current maximum of 51 A was measured. The energy deposited in the discharge and the discharge resistance were also obtained as a function of time. It resulted that 70% of the limit energy value was deposited in the first 6 ns of the discharge.

In addition to the experimental results, a full circuit simulation was performed including a discharge model resistance. The resistance is the sum of two terms, a classic Rompe and Weizel expression in series with a resistance to model the spreading of the discharge along the dielectric layer. Experiments and simulation present a good level of consistency.

The ability of the setup to expose biological cells in *in vitro* conditions and combination of nsDBD with nsPEF will be the focus of a future paper.

References

[1] J. G. Skeate, D. M. D. Silva, E. Chavez-Juan, S. Anand, R. Nuccitelli, and W. M. Kast, "Nano-Pulse Stimulation induces immunogenic cell death in human papillomavirus-transformed tumors and initiates an adaptive immune response," *PLOS ONE*, vol. 13, no. 1, p. e0191311, Jan. 2018.

[2] L. Carr, S. M. Bardet, R. C. Burke, D. Arnaud-Cormos, P. Leveque, and R. P. O'Connor, "Calcium-independent disruption of microtubule dynamics by nanosecond pulsed electric fields in U87 human glioblastoma cells," *Sci Rep*, vol. 7, p. 41267, 24 2017.

[3] S. Guo *et al.*, "Nano-pulse stimulation induces potent immune responses, eradicating local breast cancer while reducing distant metastases," *International Journal of Cancer*, vol. 142, no. 3, pp. 629–640, 2018.

[4] A. G. Pakhomov and O. N. Pakhomova, "The interplay of excitation and electroporation in nanosecond pulse stimulation," *Bioelectrochemistry*, vol. 136, p. 107598, Dec. 2020.

[5] E. B. Sözer and P. T. Vernier, "Modulation of biological responses to 2 ns electrical stimuli by field reversal," *Biochimica et Biophysica Acta (BBA) - Biomembranes*, vol. 1861, no. 6, pp. 1228–1239, Jun. 2019.

[6] R. Orlacchio, L. Carr, C. Palego, D. Arnaud-Cormos, and P. Leveque, "High-voltage 10 ns delayed paired or bipolar pulses for in vitro bioelectric experiments," *Bioelectrochemistry*, vol. 137, p. 107648, Feb. 2021.
[7] S. Kohler, V. Couderc, R. P. O'Connor, D. Arnaud-Cormos, and P. Leveque, "A versatile high voltage nano- and sub-nanosecond pulse generator," *IEEE Transactions on Dielectrics and Electrical Insulation*, vol. 20, no. 4, pp. 1201–1208, Aug. 2013.
[8] S. El Amari, A. De Angelis, D. Arnaud-Cormos, V. Couderc, and P. Leveque, "Characterization of a linear photoconductive switch used in nanosecond pulsed electric field generator," *IEEE Photonics Technology Letters*, vol. 23, no. 11, pp. 673–675, 2011.
[9] M. Soueid *et al.*, "Delivery devices for exposure of biological cells to nanosecond pulsed electric fields," *Med Biol Eng Comput*, vol. 56, no. 1, pp. 85–97, Jan. 2018.
[10] S. Kohler, R. P. O'Connor, T. D. T. Vu, P. Leveque, and D. Arnaud-Cormos, "Experimental Microdosimetry Techniques for Biological Cells Exposed to Nanosecond Pulsed Electric Fields Using Microfluorimetry," *IEEE Transactions on Microwave Theory and Techniques*, vol. 61, no. 5, pp. 2015–2022, May 2013.
[11] X. Lu, M. Laroussi, and V. Puech, "On atmospheric-pressure non-equilibrium plasma jets and plasma bullets," *Plasma Sources Science and Technology*, vol. 21, p. 034005, Apr. 2012.
[12] A. Lin *et al.*, "Uniform nanosecond pulsed dielectric barrier discharge plasma enhances anti-tumor effects by induction of immunogenic cell death in tumors and stimulation of macrophages," *Plasma Processes and Polymers*, vol. 12, no. 12, pp. 1392–1399, 2015.
[13] H. Ayan *et al.*, "Application of nanosecond-pulsed dielectric barrier discharge for biomedical treatment of topographically non-uniform surfaces," *J. Phys. D: Appl. Phys.*, vol. 42, no. 12, p. 125202, May 2009.
[14] C. Liu, A. Fridman, and D. Dobrynin, "Uniformity analysis of nanosecond and sub-nanosecond pulsed DBD in atmospheric air," *Plasma Res. Express*, vol. 1, no. 1, p. 015007, Nov. 2018.
[15] M. Malashin, S. Moshkunov, V. Khomich, and E. Shershunova, "Radial Distribution of the Nanosecond Dielectric Barrier Discharge Current in Atmospheric-Pressure Air," *Plasma Physics Reports*, vol. 44, Feb. 2018.
[16] T. Shao, P. Yan, K. Long, and S. Zhang, "Dielectric-barrier discharge excitated by repetitive nanosecond pulses in air at atmospheric pressure," *Plasma Science, IEEE Transactions on*, vol. 36, pp. 1358–1359, Sep. 2008.
[17] D. Z. Pai, D. A. Lacoste, and C. O. Laux, "Transitions between corona, glow, and spark regimes of nanosecond repetitively pulsed discharges in air at atmospheric pressure," *Journal of Applied Physics*, vol. 107, no. 9, p. 093303, May 2010.
[18] T. Shao, C. Zhang, Y. Yu, Z. Fang, and P. Yan, "Temporal evolution of nanosecond-pulse dielectric barrier discharges in open air," *EPL (Europhysics Letters)*, vol. 97, no. 5, p. 55005, Mar. 2012.
[19] V. M. Elchaninov, M. V. Shemet, and M. V. Malashin, "Dielectric barrier discharge excited by unipolar pulse voltage in submillimetric air gaps," in *2017 IEEE Conference of Russian Young Researchers in Electrical and Electronic Engineering (EIConRus)*, Feb. 2017, pp. 1135–1137.
[20] T. C. Manley, "The Electric Characteristics of the Ozonator Discharge," *Trans. Electrochem. Soc.*, vol. 84, no. 1, p. 83, Oct. 1943, doi: 10.1149/1.3071556.
[21] U. Kogelschatz, "Dielectric-barrier discharges: their history, discharge physics, and industrial applications," *Plasma Chemistry and Plasma Processing*, vol. 23, no. 1, pp. 1–46, Mar. 2003.
[22] S. Liu and M. Neiger, "Excitation of dielectric barrier discharges by unipolar submicrosecond square pulses," *J. Phys. D: Appl. Phys.*, vol. 34, no. 11, pp. 1632–1638, Jun. 2001.
[23] S. Liu and M. Neiger, "Electrical modelling of homogeneous dielectric barrier discharges under an arbitrary excitation voltage," *Journal of Physics D: Applied Physics*, vol. 36, no. 24, p. 3144, 2003.
[24] T. Shao *et al.*, "Electrical characterization of dielectric barrier discharge driven by repetitive nanosecond pulses in atmospheric air," *Journal of Electrostatics*, vol. 67, no. 2, pp. 215–221, May 2009.
[25] S. Bhosle, G. Zissis, J. J. Damelincourt, and F. P. Dawson, "Calculation of the impedance of an axisymetric DBD lamp for power supply design purposes," in *Conference Record of the 2004 IEEE Industry Applications Conference, 2004. 39th IAS Annual Meeting.*, Oct. 2004, vol. 3, pp. 1667–1670.
[26] N. Naudé, J.-P. Cambronne, N. Gherardi, and F. Massines, "Electrical model of an atmospheric pressure townsend-like discharge (APTD)," *Eur. Phys. J. Appl. Phys.*, vol. 29, no. 2, Art. no. 2, Feb. 2005.
[27] R. Jobava *et al.*, "Computer simulation of ESD from voluminous objects compared to transient fields of humans," *IEEE Transactions on Electromagnetic Compatibility*, vol. 42, no. 1, pp. 54–65, Feb. 2000.
[28] M. Kenaan *et al.*, "Characterization of a 50- Ω exposure setup for high-voltage nanosecond pulsed electric field bioexperiments," *IEEE Trans Biomed Eng*, vol. 58, no. 1, pp. 207–214, Jan. 2011.
[29] D. Bessières, J. Paillol, and N. Soulem, "Negative corona triggering in air," *Journal of Applied Physics*, vol. 95, no. 8, pp. 3943–3951, Mar. 2004.
[30] M. Bouzidi, X. Bonnin, N. Naudé, H. Piquet, A. Belinger, and N. Gherardi, "Maximization of the working domain of an Atmospheric Pressure Townsend Discharge (APTD) using a current-source static converter," *Journal of Physics: Conference Series*, vol. 550, p. 012044, Nov. 2014.
[31] D. Arnaud-Cormos, S. Kohler, D. Bessières, R. P. O'Connor, J. H. Paillol, and P. Lévêque, "Electrical measurements for nanosecond repetitive pulsed discharge," *IEEE Transactions on Plasma Science*, vol. 42, no. 7, pp. 1909–1916, Jul. 2014.
[32] E. Anderson *et al.*, *LAPACK users' guide: third edition*. SIAM, 1999.
[33] F. Wan, V. Pilla, J. Li, D. Pommerenke, H. Shumiya, and K. Araki, "Time lag of secondary ESD in millimeter-size spark gaps," *IEEE Transactions on Electromagnetic Compatibility*, vol. 56, no. 1, pp. 28–34, Feb. 2014.
[34] J. Laimer and H. Störi, "Glow discharges observed in capacitive radio-frequency atmospheric-pressure plasma jets.," *Plasma Processes Polym.*, vol. 3, no. 8, pp. 573–586, Oct. 2006.
[35] J. Schulze, E. Schüngel, Z. Donkó, and U. Czarnetzki, "The electrical asymmetry effect in multi-frequency capacitively coupled radio frequency discharges," *Plasma Sources Science and Technology*, vol. 20, no. 1, p. 015017, 2011.
[36] A. Belasri, J. P. Boeuf, and L. C. Pitchford, "Cathode sheath formation in a discharge-sustained XeCl laser," *Journal of Applied Physics*, vol. 74, no. 3, pp. 1553–1567, Aug. 1993.
[37] S. Bonisch, W. Kalkner, and D. Pommerenke, "Modeling of short-gap ESD under consideration of different discharge mechanisms," *IEEE Transactions on Plasma Science*, vol. 31, no. 4, pp. 736–744, Aug. 2003.
[38] J. M. Meek, and J. D. Craggs, "Electrical Breakdown of Gases". Clarendon, Oxford, eds., 1953.
[39] D. Pommerenke, "ESD: transient fields, arc simulation and rise time limit," *Journal of Electrostatics*, vol. 36, no. 1, pp. 31–54, Nov. 1995.
[40] F. Tholin and A. Bourdon, "Simulation of the hydrodynamic expansion following a nanosecond pulsed spark discharge in air at atmospheric pressure," *J. Phys. D: Appl. Phys.*, vol. 46, no. 36, p. 365205, Aug. 2013.
[41] T. W. Hussey, K. J. Davis, J. M. Lehr, N. F. Roderick, R. C. Pate, and E. Kunhardt, "Dynamics of nanosecond spark-gap channels," in *Digest of Technical Papers. 12th IEEE International Pulsed Power Conference. (Cat. No.99CH36358)*, Jun. 1999, vol. 2, pp. 1171–1174 vol.2.
[42] M. Istenič, I. Smith, and B. Novae, "Dynamic resistance calculation of nanosecond spark-gaps," *2005 IEEE Pulsed Power Conference*, 2005.

Martinus Dobbelaar was born in Nieuwegein, The Netherlands, in 1983. He received a bachelor degree in mathematics in 2007, a bachelor degree in chemistry in 2012 and a master degree in physics in 2014 from the Utrecht University, Utrecht, The Netherlands. He received the Ph.D. degree with the University of Pau, Pau, France and the XLIM Research Institute, Limoges, France in 2017. His current research interests include the development and characterization of exposure setups to study the effect of nanosecond electromagnetic fields and discharges on complex media.

Delphine Bessieres was born in Tarbes, France, in 1979. She received the PhD degree from the University of Pau, France, in 2006. Since 2007, she is an Associate Professor at the University of Pau, Laboratoire des Sciences de l'Ingénieur Appliquées à la Mécanique et au Génie Electrique (SIAME laboratory). Her research interests concern the modeling and the numerical simulation of plasma discharges at atmospheric pressure.

Delia Arnaud-Cormos (M'05) was born in Cugir, Romania, in 1978. She received the Diplôme d'Ingénieur degree from the Institute of Computer Science and Communication, Rennes, France, in 2002, and the master's and Ph.D. degrees from INSA, Rennes, in 2003 and 2006, respectively. Since 2007, she has been with the Bioelectromagnetics Team, XLIM Institute, University of Limoges/C.N.R.S., Limoges, France, as an Associate Professor. In 2012, she joined the Pulsed Power Group, University of Southern California (USC), Los Angeles, SC, USA, where she developed research with the Biological Applications Research Team. Since 2018, she has been a Junior Member with the Institut Universitaire de France (IUF), Paris, France, and a member of the International Bioelectrics Consortium. Her current research interests include nanosecond pulses/microwave exposure system setup and dosimetric characterization for bioelectromagnetic studies.

Philippe Leveque (M'03) was born in Poitiers, France, in 1964. He received the Ph.D. degree from the University of Limoges, Limoges, France, in 1994. In 1995, he joined C.N.R.S. He is involved in the development of dosimetry and exposure setups for health-risk assessment in cooperation with biological and medical research groups. He is currently a Senior Scientist with CNRS and the Group Leader of Bioelectromagnetics Team with the XLIM Research Institute focusing on nanopulse application. His current research interest includes the scattering problems of electromagnetic waves, particularly in the time domain.

Jean Paillol was born in Brive, France, in 1965. He received the Ph.D. degree from the University of Limoges, France in 1993. In 1993, he joined the University of Pau as an Assistant Professor, and a professor since 2016. His research concerns the fundamental physical phenomena in electrical discharges at atmospheric pressure and numerical simulation.